Kinetic Evidence Supports the Existence of Two Halide Binding Sites that Have a Distinct Impact on the Heme Iron Microenvironment in Myeloperoxidase†

Gheorghe Proteasa,‡ Yahya R. Tahboub,‡ Semira Galijasevic,‡ Frank M. Raushel,§ and Husam M. Abu-Soud*,‡,||

Department of Obstetrics and Gynecology, The C. S. Mott Center for Human Growth and Development, and Department of Biochemistry and Molecular Biology, Wayne State University School of Medicine, Detroit, Michigan 48201, and Department of Chemistry, Texas A&M University, College Station, Texas 77842

Received May 16, 2006; Revised Manuscript Received October 11, 2006

ABSTRACT: Myeloperoxidase (MPO) structural analysis has suggested that halides and pseudohalides bind to the distal binding site and serve as substrates or inhibitors, while others have concluded that there are two separate sites. Here, evidence for two distinct binding sites for halides comes from the bell-shaped effects observed when the second-order rate constant of nitric oxide (NO) binding to MPO was plotted versus Cl^- concentration. The chloride level used in the X-ray structure that produced Cl^- binding to the amino terminus of the helix halide binding site was insufficient to populate either of the two sites that appear to be responsible for the two phases. Biphasic effects were also observed when the I^-, Br^-, and SCN^- concentrations were plotted against the NO combination rate constants. Interestingly, the trough concentrations obtained from the bell-shaped curves are comparable to normal plasma levels of halides and pseudohalides, suggesting the potential relevance of these molecules in modulating MPO function. The second-order rate constant of NO binding in the presence of plasma levels of I^-, Br^-, and SCN^- is 1−2-fold lower compared to that obtained in the absence of these molecules and remains unaltered through the Cl^- plasma level. When Cl^- exceeded the plasma level, the NO combination rate becomes indistinguishable from the second phase of the bell-shaped curve that was obtained in the absence of halides. Our results are consistent with two halide binding sites that could be populated by two halides in which both display distinct effects on the MPO heme iron microenvironment.

Myeloperoxidase (MPO)[1] is an abundant heme-containing protein found in neutrophil granules, monocytes, and selected tissue macrophages (*1*−*3*). MPO plays an important role in generating an array of toxic oxidants important to host defense (*1*−*3*). The molecular mass of the enzyme is 150−165 kDa and the enzyme is comprised of two identical subunits joined by a single disulfide bridge (*2*). Each subunit consists of a light chain and a heavy chain derived from a single gene product (*4*). The heavy chains contain an iron bound to a novel protoporphyrin IX derivative that is covalently attached to the heavy chain polypeptide (*5*, *6*). The heme prosthetic groups are approximately 50 Å apart, and a variety of observations suggest that both are functionally identical (*7*−*10*). They presumably operate independently in the oxidation of Cl^- and in the bactericidal activity of the enzyme (*7*). Structural studies of both canine and human MPO demonstrate that the heme of MPO is positioned at the base of a deep and narrow cleft and is axially coordinated to the protein through His933 (*7*−*10*). The imidazole ring of His95 is located 5.7 Å from the heme iron, while the guanidinium group of Arg239 and the side chain of Gln91 are close to the heme surface and have minimum interatomic distances from the iron atom of 7.0 and 4.5 Å, respectively (*7*−*10*). The location of these residues above the heme iron is consistent with the heme iron being the site where hydrogen peroxide (H_2O_2) binds and becomes activated in MPO so that the intermediate Compound I can react directly with the halides.

Oxidation of the ferric MPO by H_2O_2 generates MPO Compound I, a ferryl π cation radical [MPO−Fe(IV)═$O^{\bullet+\pi}$]. This process is associated with activation of synthesis of hypohalous acid from halides and pseudohalides, or with the production of radical species and the MPO intermediate Compound II [MPO−Fe(IV)═O] from one-electron substrates, such as superoxide ($O_2^{\bullet-}$) and ascorbic acid (*11*, *12*). Reduction of Compound II to the ferric state is thought to be the rate-limiting step in the classic peroxidase cycle, and this step can be accelerated by physiological reductants like $O_2^{\bullet-}$, nitric oxide (NO), and ascorbic acid (*12*−*17*). Previously, we have demonstrated that NO modulates the catalytic activity of mammalian heme peroxidases by serving as a substrate or a ligand (*15*−*19*). High levels of NO are inhibitory via the formation of a stable six-coordinate low-spin nitrosyl complex with the ferric heme, whereas low levels of NO accelerate the overall rate of the peroxidase

† This work was supported by a grant from the National Institutes of Health (HL066367, H.M.A.-S.) and by an award from the American Heart Association (S.G.).

* To whom correspondence should be addressed: Department of Obstetrics and Gynecology, The C. S. Mott Center for Human Growth and Development, Wayne State University School of Medicine, 275 E. Hancock, Detroit, MI 48201. Telephone: (313) 577-6178. Fax: (313) 577-8554. E-mail: habusoud@med.wayne.edu.

‡ Department of Obstetrics and Gynecology, The C. S. Mott Center for Human Growth and Development, Wayne State University School of Medicine.

§ Texas A&M University.

|| Department of Biochemistry and Molecular Biology, Wayne State University School of Medicine.

[1] Abbreviations: Br^-, bromide; Cl^-, chloride; H_2O_2, hydrogen peroxide; I^-, iodide; MPO, myeloperoxidase; NO, nitric oxide (nitrogen monoxide); SCN^-, thiocyanate.

10.1021/bi0609725 CCC: $37.00 © 2007 American Chemical Society
Published on Web 12/15/2006

cycle via reduction of Compounds I and II (*15*−*17*). We have also shown that the MPO/H_2O_2 system upregulates the catalytic activity of inducible nitric oxide synthase (iNOS) by scavenging NO, thus preventing feedback inhibition attributed to the formation of an iNOS−Fe−NO complex (*17*).

Human MPO crystal structures of the cyanide complex and its interaction with bromide and thiocyanate have been shown to be a useful analogue of Compound I for studies of the halide substrate binding (*10*). The structure of the MPO−chloride complex identified Cl^- at the amino terminus of the helix containing the proximal His336 (*9*). In contrast, structural studies of MPO-bound SCN^- and Br^- show in detail how these substrates bind in the distal and proximal cavity, which replace a water molecule (W2) and are hydrogen bonded to the side chain of Gln91 (*10*). Two additional Br^- atoms are also located on the surface of the protein, relatively far from the heme (*10*). Importantly, these structural analyses do not exclude the possibility that there are two separate sites on MPO for halide binding as a substrate and as an inhibitor (*10*).

To investigate what role halides and pseudohalides play in reshaping the MPO heme pocket architecture, we utilized rapid kinetic measurements to study reactions of the ferric heme iron with NO. This report provides evidence that preincubation of MPO with halides and pseudohalides generates or unmasks two additional MPO binding sites for halides and pseudohalides.

MATERIALS AND METHODS

Materials. NO gas was purchased from Matheson Tri-Gas Products, Inc. (Montgomeryville, PA) and used without further purification. For each experiment, a fresh saturated stock of NO was prepared under anaerobic conditions. The extent of nitrite/nitrate (NO_2^-/NO_3^-) buildup in NO preparations over the time course used for the present studies was <1−1.5% (per mole of NO), as determined by anion exchange HPLC under anaerobic conditions (*20*). All other reagents and materials were of the highest-purity grades available and obtained from Sigma Chemical Co. (St. Louis, MO), or the indicated source.

General Procedures. MPO was initially purified from detergent extracts of human leukocytes by sequential lectin affinity and gel filtration chromatography (*21*). Trace levels of contaminating eosinophil peroxidase (EPO) were then removed by passing the samples over a sulfopropyl Sephadex column (*22*). The purity of isolated MPO was established by demonstrating a Reinheitzal (RZ) value of >0.85 (A_{430}/A_{280}), SDS−PAGE analysis with Coomassie Blue staining, and gel tetramethylbenzidine peroxidase staining to confirm no contaminating EPO activity. Enzyme concentration was determined spectrophotometrically utilizing extinction coefficients of 89 000 M^{-1} cm^{-1} per heme of MPO (*23*). The concentration of the MPO dimer was calculated as half the indicated concentration of the heme-like chromophore (*24*).

Optical Spectroscopy and Rapid Kinetic Measurements. Optical spectra were recorded on a Cary 100 Bio UV−visible spectrophotometer, at 25 °C. Anaerobic spectra of MPO forms were recorded using septum-sealed quartz cuvettes that could attach through a quick-fit joint to a vacuum system. The peroxidase samples were made anaerobic by repeated cycles of evacuation and equilibrated with catalyst-deoxygenated N_2. Cuvettes were maintained under a N_2 or NO atmosphere during spectral measurements. All kinetic measurements were performed with a temperature-controlled dual-syringe stopped-flow instrument obtained from Hi-Tech, Ltd. (model SF-61). Experiments were initially performed under conditions identical to those recently reported for MPO (*15*−*19*) to facilitate comparisons. Measurements were carried out under an anaerobic atmosphere at 10 °C following rapid mixing of equal volumes of the enzyme solutions (0.86 μM) supplemented with increasing halide or pseudohalide concentrations against buffer solution supplemented with increasing concentrations of NO. The reactions for NO binding to the MPO−Fe(III) species were monitored by following the decrease at 430 nm. To determine the apparent rate constants for the formation of the MPO−Fe(III)·NO complex, the time course of absorbance change was fit to a single-exponential function ($Y = 1 - e^{-kt}$) using a nonlinear least-squares method provided by the instrument manufacturer. Signal-to-noise ratios for all kinetic analyses were improved by averaging at least six to eight individual traces.

Solution Preparation. A fresh saturated stock of NO was prepared under anaerobic conditions. Anaerobic 0.2 M sodium phosphate buffer solutions (pH 7.0) containing various concentrations of NO were prepared by mixing different volumes of buffer saturated with NO gas at 21 °C with an anaerobic buffer solution. A saturating concentration of NO at 21 °C is approximately 2 mM.

Preparation of MPO Crystal Structure Figures. The figures were produced using coordinate files from the Protein Data Bank (entry 1DNW and entry 1MHL for Figure 5 and entry 1D7W for Figure 6) and as visualization program PyMOL (DeLano Scientific, LLC, San Carlos, CA).

RESULTS

Formation, Stability, and Reversibility of the MPO−Fe(III)·NO Complex. Soret and visible regions of the absorbance spectra of the enzyme are sensitive to microscopic changes in heme pocket geometry and electronic environment when the ligand binds to the ferric form of MPO. Indeed, spectroscopic studies demonstrated that addition of NO to the ferric human MPO [MPO−Fe(III)] produced a decrease in absorbance and a shift in the Soret region of the heme from 430 to 433 nm, as well as an additional absorbance peak in the visible range at 630 nm, as previously reported (*18*, *19*). These results demonstrate that NO binds to MPO and forms a low-spin six-coordinate Fe(III)·NO complex. No further spectral changes were observed after 30 min under anaerobic conditions, indicating that the MPO−Fe(III)·NO complex is stable. Degassing NO under anaerobic conditions restored the original spectrum, indicating the reversible nature of this complex. Spectral evidence also suggested that NO binds to MPO−Fe(III) in the absence and presence of Cl^- at high and low pH (pH 3−9), but the subsequent stability of this complex depended on the experimental conditions.

Stopped-Flow Analysis of Binding of NO to Human MPO. The halides and pseudohalides bind to the MPO distal binding site and serve as a substrate or inhibitor and modulate the heme iron microenvironment. They cause significant alteration in the catalytic site, thereby altering the affinity of the enzyme for H_2O_2 (*25*, *26*). Because the formation of Compound I is slower than the two-electron oxidation of halide, the accumulation of Compound I cannot be detected

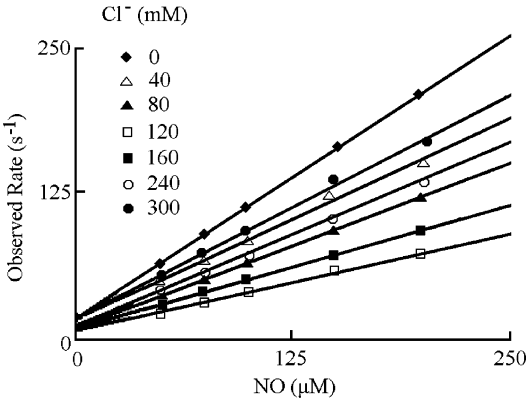

FIGURE 1: Cl^- modulates binding of NO to MPO heme iron. Plots of the observed rates of binding of NO to MPO−Fe(III) as a function of NO and Cl^- concentrations. An anaerobic solution containing 0.86 μM MPO−Fe(III) supplemented with varying concentrations of Cl^- was rapidly mixed with an equal volume of sodium phosphate buffer (200 mM at pH 7.0) supplemented with varying concentrations of NO, at 10 °C. The high concentration of the phosphate buffer keeps the solution pH unaltered after the addition of NO. The observed rates of the MPO−Fe(III)·NO complex were plotted as a function of NO concentration. The standard error for each individual rate constant has been estimated to be less than 10%.

during steady state catalysis (*26*, *27*). Therefore, the influence of the preincubation of halides with MPO on H_2O_2 binding to the enzyme cannot be measured directly using standard methods.

To assess the effect of halides and pseudohalides on binding of ligand and substrate to the catalytic sites of MPO, we examined the rate of binding of NO to the heme moiety of the peroxidase. This process emphasized the influence of cosubstrate binding on the microenvironment of the catalytic site of MPO and the influence on ligand and substrate binding. Stopped-flow methods were used to determine the combination (k_{on}) and dissociation rates (k_{off}) for binding of NO to the Fe(III) form of MPO. Experiments were performed under two different conditions: (1) rapid mixing of native MPO preincubated with an increasing halide concentration with a solution supplemented with a fixed amount of NO and (2) rapid mixing of a native MPO preincubated with a fixed halide concentration supplemented with increasing amounts of NO. Initial experiments were focused on the formation of the MPO−Fe(III)·NO complex. The concentrations of NO, halides, and pseudohalides employed were in large molar excess of MPO to ensure pseudo-first-order conditions. The apparent rate constants obtained for the interaction between MPO−Fe(III) and NO were plotted against either Cl^- (when the NO concentration was fixed) or NO (when the Cl^- concentration was fixed) concentrations to obtain the first- and second-order rate constants for the reactions. In all cases, the plots of the apparent rate constants for NO binding as a function of NO concentration were linear, consistent with a simple one-step mechanism (Figure 1). Similar behavior was obtained when Cl^- was replaced with I^-, Br^-, and SCN^- (data not shown). The positive intercepts confirm that NO binds to MPO−Fe(III) by a reversible process, as shown in eq 1.

$$\text{MPO}-\text{Fe(III)} + \text{NO} \underset{k_{off}}{\overset{k_{on}}{\rightleftharpoons}} \text{MPO}-\text{Fe(III)}\cdot\text{NO} \qquad (1)$$

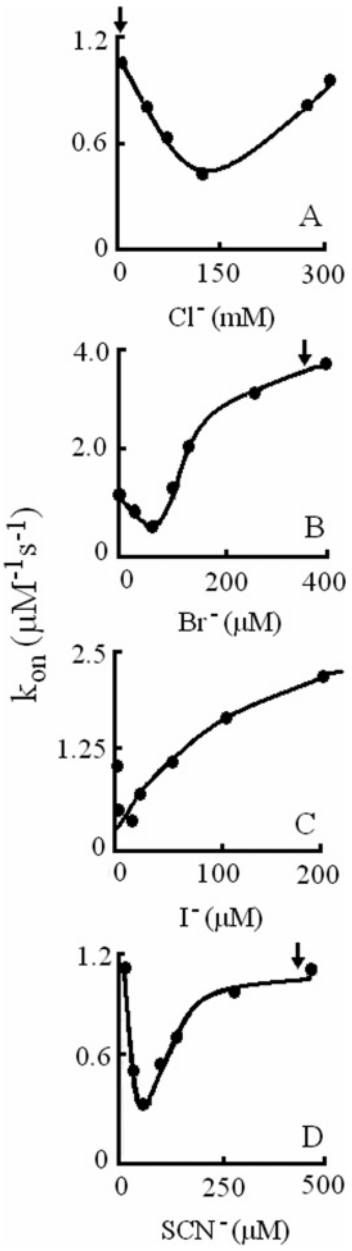

FIGURE 2: Relationship between the second-order combination rate constant (k_{on}) for binding of NO to MPO−Fe(III) as a function of Cl^- (A), Br^- (B), I^- (C), and SCN^- (D) concentration. Experiments were carried out at 10 °C using stopped-flow methods. For comparison, arrows indicate halides concentration used for crystallization of MPO by Fenna and co-workers (*7*−*10*). The standard error for each individual rate constant has been estimated to be less than 10%.

Biphasic effects were observed when the second-order combination rate constants (k_{on}) of NO binding calculated from the slopes were plotted as a function of Cl^-, I^-, Br^-, and SCN^- concentration (Figure 2). Biphasic effects were also observed when the first-order dissociation rate constants (k_{off}) of NO binding calculated from the intercepts were plotted as a function of Cl^-, I^-, Br^-, and SCN^- concentration (Figure 3). Kinetics may indicate that halides and pseudohalides bind at two different sites of MPO and both sites have a distinct effect on the MPO heme iron microenvironment.

To confirm the existence of two separate binding sites and to determine what effect the binding to one site has on the

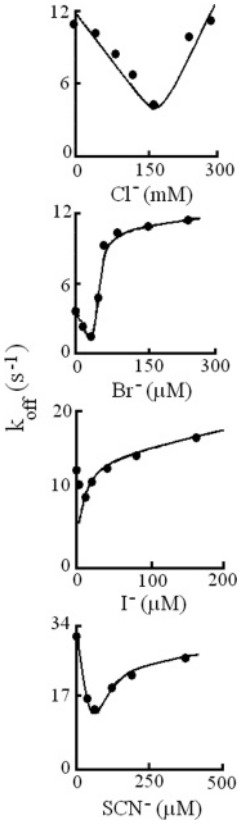

FIGURE 3: Relationship between the first-order dissociation rate constant (k_{off}) of binding of NO to MPO−Fe(III) as a function of Cl^-, Br^-, I^-, and SCN^- concentration. Experiments were carried out at 10 °C using stopped-flow methods. The standard error for each individual rate constant has been estimated to be less than 10%.

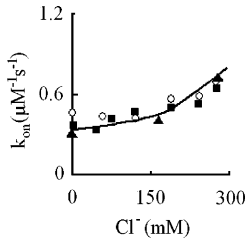

FIGURE 4: Relationship between the second-order combination rate constant (k_{on}) for binding of NO to MPO−Fe(III) as a function of Cl^- concentration when MPO was incubated with 80 μM Br^- (○), when MPO−Fe(III) was incubated with 5 μM I^- (■), and when MPO−Fe(III) was incubated with 75 μM SCN^- (▲). Experiments were carried out at 10 °C. The standard error for each individual rate constant has been estimated to be less than 10%.

other, the experiments described above were repeated with some modifications. MPO solutions supplemented with a fixed amount of Br^-, I^-, or SCN^- (e.g., plasma level) and increasing Cl^- concentrations were rapidly mixed against a buffer solution supplemented with increasing concentrations of NO, under anaerobic conditions. The second-order combination rate constants of NO binding were obtained and plotted against the Cl^- concentration. As shown in Figures 2 and 4, the second-order rate constant of NO binding in the presence of plasma levels of I^-, Br^-, and SCN is 1−2-fold lower compared to that obtained in the absence of these molecules and remains unaltered throughout the Cl^- plasma levels. When the Cl^- concentration exceeded the plasma levels, the NO combination rate became indistinguishable

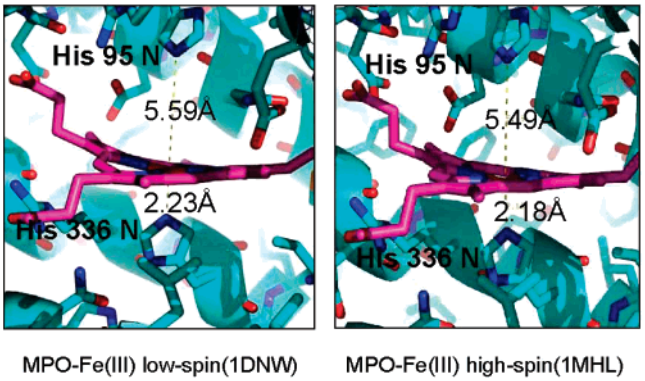

FIGURE 5: Differences in the heme pocket microenvironment of the low-spin (left) and the high-spin (right) heme iron crystal structures of MPO.

from the upward slope of the second phase of the biphasic curve that is obtained in the absence of I^-, Br^-, and SCN^-. Our results are consistent with two halide binding sites that can accommodate two chloride atoms, or one chloride and the other Br^-, I^-, or SCN^-.

DISCUSSION

Analysis of crystal structures by Fenna and co-workers has suggested that halides and pseudohalides bind to the distal site of MPO and serve as substrates or inhibitors (*7*−*10*). However, these MPO crystal structure analyses do not exclude the possibility of the existence of two separate halide binding sites. Earlier studies by several groups have concluded that there are two separate sites on MPO for the binding of halides as substrates and inhibitors (*27*−*30*). The two-binding site hypothesis for halides comes from the biphasic effects observed when the second-order rate constant for binding of NO to MPO was plotted against the Cl^- concentration (Figure 2A). The concentration of chloride used in the X-ray structure (2 mM Cl^-) (*7*−*10*) was insufficient to populate either of the two sites that appear to be responsible for the two phases that are illustrated in Figure 2A. The Cl^- concentration of 2 mM enabled binding of Cl^- to the amino terminus of the helix halide binding site (*7*−*10*). Because of the remote location from the heme and the existence of two α-helices longitudinally positioned between this site and the heme pocket, the proximal helix halide binding site appears unlikely to be involved in a way that alters the heme iron microenvironment. Biphasic effects have also been observed when the SCN^-, I^-, and Br^- concentrations were plotted against the second-order rate constants for binding of NO to MPO (Figure 2B−D). Crystallographic studies of MPO have indicated that the concentrations of Br^- or SCN^- used in the crystal structure appear to be sufficiently high for population of both the proximal and distal sites (*7*−*10*). Indeed, it was high enough to facilitate binding of two additional Br^- atoms on the surface of MPO, each 25 Å from the heme iron center (*7*−*10*).

The core size of MPO heme is affected by the oxidation and spin states of the central Fe ion and by the nature of the axial ligands (Figure 5). Recent studies by Araki and Takeuchi (*31*) on the effects of pH and Cl^- concentration on the structure of the MPO heme moiety utilizing resonance Raman spectroscopy have indicated the existence of two forms of MPO: an alkaline (high-spin) form and an acidic

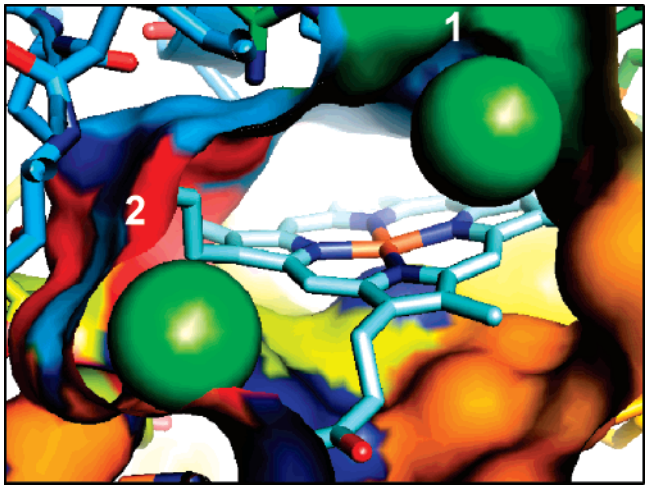

FIGURE 6: Possible binding sites for the two Cl^- atoms (1 and 2) in the heme pocket. The first Cl^- may bind to the first site in the distal pocket in a crevice created by Arg239 (CG), Phe336 (CZ), and Glu242 (CA), while the second Cl^- may bind to a pocket nestled among residues Arg333 (NH2), Asn330 (CA), and Thr239 (CB). This figure was generated using coordinates from PDB entry 1D7W in the PyMOL protein viewing program.

(low-spin) form. In their studies, the authors have shown that the alkaline form was predominant at neutral pH, and with an increase in Cl^- concentration, the equilibrium was shifted from the alkaline to the acidic form. This shift in MPO population is associated with a significant alteration in the structure of the heme itself and of the protein moiety around the heme, as judged by the appearance and the downshift of the ν(Fe−His) mode in the resonance Raman spectra (*31*). These structural alterations in MPO are consistent with the MPO pocket being able to accommodate two Cl^- atoms. The apparent ability of the MPO heme pocket to accommodate two Cl^- atoms is unprecedented, and it may reveal how Cl^- binding completes the catalytic cycle for synthesis of the essential biological cytotoxin HOCl. MPO is in the ferric high-spin state at neutral pH.

The Cl^- ion used in HOCl production may bind to the first site in the distal pocket in a crevice created by Arg239 (CG), Phe336 (CZ), and Glu242 (CA) (Figure 6). This Cl^- ion displays a higher affinity for the enzyme but does not alter the oxidation and spin states. Binding of the second Cl^- to the heme pocket likely occurs in a hydrophobic pocket nestled among residues Arg333 (NH2), Asn330 (CA), and Thr239 (CB). This binding allows the distal pocket to generate low-spin heme iron by pressuring the pyrrole ring IV(A) to tilt and expose a heme edge to the adjacent CAA and C2A atoms of the pyrrole ring for Cl^- interaction. This modification, subsequently, weakens the Fe−His336 linkage which allows the displacement of the Fe ion from His336 to the center of the porphyrin ring and creates a 5.59 Å wide open active center channel (increased by 0.1 Å compared to that of the high-spin form) (Figure 5, left). This transition has been characterized utilizing resonance Raman spectroscopy by following the Fe−His vibration shifts from 220 cm^{-1} in the alkaline form to 218 cm^{-1} in the acidic form (*31*). Interactions of heme pyrrole with the second Cl^- atom suggest that this Cl^- has electronic influences on the heme-bound H_2O_2. Cl^- binds to and stacks with the heme in an otherwise hydrophobic pocket to aid in activation of the heme-bound oxygen by direct proton donation and thereby differentiates the two chemical steps for HOCl synthesis. When HOCl is generated, the second Cl^- atom moves to replace the first one. This course of action is likely accompanied by a strengthening of the Fe−His336 linkage which may allow the Fe ion to move away from the porphyrin ring center and closer to His336. Indeed, the Fe−His336(N) distance decreased from 2.23 Å in the low-spin form to 2.18 Å in the high-spin form (Figure 5, right). This narrowing of the heme pocket may cause the expulsion of the HOCl molecule. Higher Cl^- concentrations may increase the affinity of MPO for Cl^-, cease the pyrrole ring movement, and keep MPO in its inactive form in catalyzing HOCl production. Higher Cl^- concentrations also appear to broaden the access of NO to the ferric heme iron, allowing NO to bind unhindered as mirrored by the increase in the rate of NO binding at higher Cl^- concentrations. The fact that this does not occur in other hemoprotein model compounds indicates that MPO is a unique heme−nitrogen protein in this respect.

A growing body of evidence has suggested that hydrogen bonding and cosubstrate interaction play a contributory and even predominant role in ligand discrimination by MPO. Previous studies by Bolscher and Wever have suggested the existence of one halide binding site. In their system, they have demonstrated that there is an acid/base group on MPO (with a pK_a of 4.30) which, when protonated, appeared to restrict the access of flexible bulky molecules (i.e., H_2O_2) and small rigid molecules (i.e., CN) to the ferric heme iron (*32*). NO is a diatomic flexible ligand that displays the potential capacity to adopt a bent geometry in hemoproteins and binds MPO to form a low-spin six-coordinate complex. Evidence obtained with sterically unhindered heme model compounds (*33*) and heme proteins, such as hemoglobin A (*34*) or cytochrome *c* oxidase (*35*), showed that a bent Fe−NO bond is preferred. X-ray studies with model porphyrins and heme proteins indicate that Fe−CN complexes are more rigid than Fe−NO complexes and, consequently, occupy more space (*10*, *36*, *37*). The binding of CN to a sterically restricted form of MPO should be more difficult than that observed for NO. Thus, H_2O_2 like NO, but unlike CN, adopts a more bent geometry when bound to heme iron in the MPO ground state prior to the formation of Compound I. Our data indicate that the rapid rate of NO binding in the absence of a cosubstrate is consistent with this form of MPO containing a relatively open distal pocket that allows NO to bind unhindered. Protonation and/or cosubstrate binding to the acid base site of MPO may constrain NO binding either by filling the space directly above the heme moiety or by causing a protein conformational change that constricts the distal heme pocket. Forcing a diatomic ligand such as NO to adopt a bent geometry in hemoprotein is thought to lower its binding affinity (*38*−*40*). This would explain our observation of a decrease in the NO combination rates with an increase in substrate concentration to plasma levels.

The rate of dissociation of NO from its respective six-coordinate MPO complex was fast when compared with those of other hemoproteins (*18*, *38*, *39*, *41*), but it could be attenuated with an increase in halide concentration to plasma levels. A slower NO dissociation rate constant is thought to be due to a positive trans effect contributed by the proximal ligand which, in this case, is a histidine nitrogen. The spontaneous increase in both the association and dissociation

rate constants with an increase in Cl^- levels indicates the presence of the second Cl^- binding site (Figure 6). A steric effect on the second Cl^- binding that allows the heme to tilt through its interaction with the CAA ring that caused an alteration in the His−Fe bond is easy to imagine (Figures 5 and 6) (*42*). Such an effect may, subsequently, cause a protein conformational change that releases the restriction of NO binding to the heme iron and alters the His−Fe bond. This behavior is an exceptional case among other hemoprotein model compounds in which binding of halides to MPO has a dual effect on the MPO heme iron microenvironment and explains why halides had the same effect on k_{on} and k_{off} for binding of NO to myeloperoxidase. This explanation fits our proposed model in which the conversion of MPO from high-spin to low-spin mode and vice versa is associated with the modulation of the His−Fe bond distance. Collectively, the dual regulation of MPO ligand binding by the cosubstrates, halides and pseudohalides, represents a new means by which MPO catalytic activity can be controlled by substrate binding. Our halide binding data indicate that Cl^-, Br^-, I^-, and SCN^- play an important role in shaping the distal heme pocket in MPO and suggest that in the absence of these cosubstrates, the distal pocket may minimally restrict access of the ligand to the heme.

Our spectral evidence suggests that NO binds to MPO−Fe(III) in the absence and presence of Cl^- at high and low pH. Thus, the Bolscher and Wever system was limited by the strong double bond between C and N atoms, the inflexibility of the C−N bond, the high affinity of CN for MPO−Fe(III), and their subsequent effect on the trans Fe−His bond. These were the main reasons for Bolscher and Wever to suppose that there was one complex of MPO with halides and pseudohalides (*32*).

Of additional interest is the observation that the trough of the biphasic curves shown in Figure 2 is comparable to normal plasma levels [100 mM Cl^-, 50−150 μM Br^-, 0.1−0.6 μM I^-, and 20−120 μM SCN^- (*43*−*45*)]. The alteration in the biphasic curves and the shift in the trough concentrations indicate that these cosubstrates display distinct effects on the heme iron microenvironment. This is expected, since these cosubstrates have different physical and chemical properties, ion size, electronegativity, and affinity for MPO. Given the radius and charge of Br^- compared to Cl^-, the polarizability of this halide is higher than that of the Cl^-, which may explain why the association rate constant for binding of NO to MPO in the presence of bromide is greater than in the presence of chloride (*46*). Two binding sites for Cl^- were previously suggested by Andrews and Krinsky, who utilized tetramethylbenzidine to examine the effect of pH, H_2O_2, and Cl^- on the activity of MPO (*27*). This orientation facilitates the transfer of electrons to the heme iron and the inclusion of the ferryl oxygen into the hypohalous acid derived from the reaction (*7*−*10*). The catalytic role of the distal histidine would be dual. The first step would be the acceptance of a proton from H_2O_2 just before the scission of the O−O bond. It will be followed by a second step in which the halide substrate is oriented with respect to the heme iron in such a manner so that is accessible for electron transfer to Compound I (*7*−*10*). Andrews and Krinsky have shown that binding of Cl^- to the inhibitor binding site requires the prior protonation of this site, as the effect of altering H_2O_2 binding is only observed at acidic pH (*27*). The structural orientation, the distinguishing functional properties, and the factors that allow Compound I formation in solution are currently being investigated.

Investigation of the three-dimensional structures for a number of peroxidases (CCP, AP, LiP, and MnP) identified the existence of two binding sites within the heme pocket, a distal H_2O_2 binding pocket formed by the Arg-Trp/Phe-His sequence, and a proximal heme iron ligand pocket represented by His-Trp/Phe/Leu-Asp (*47*−*53*). On the basis of our kinetic measurements, it is, therefore, perfectly conceivable to assume that the human MPO, which is greatly similar with CCP, AP, LiP, and MnP, will benefit from the same dual heme pocket binding site configuration (*47*−*53*).

Our results are consistent with two halide binding sites on MPO that could be populated by two Cl^- atoms, or by one Cl^- and the other by Br^-, I^-, or SCN^-. Our data also support the notion that Br^-, I^-, and SCN^- display higher affinities for the first binding site of MPO, and these molecules cannot be replaced with Cl^-. Previous studies have demonstrated that the bound chloride ion at the proximal His336 site can be replaced with Br^- (*7*−*10*).

Collectively, preincubation of MPO with halides and pseudohalides generates a complex biological setting and suggests the possibility of the existence of two separate binding sites for halides. Thus, preincubation of MPO with its cosubstrate, halides and pseudohalides, may cause conformational changes that alter the reactivity of the heme iron and may generate or unmask an additional MPO binding site for halides or pseudohalides. Therefore, any structural changes in the MPO heme environment that arise due to binding of the cosubstrate to the active and inactive sites or to MPO heme reduction are envisioned to potentially affect the heme iron environment, its substrate binding, its reduction potential, and its catalytic activity. This may provide new insights into the biological role of MPO, particularly in organs that experience a range of pH and levels of halides and pseudohalides, such as the lung of asthmatic patients and smokers (*54*, *55*).

ACKNOWLEDGMENT

We are grateful to Dr. Bettie Sue Masters for her helpful comments and suggestions during the performance of this study.

REFERENCES

1. Klebanoff, S. J. (2005) Myeloperoxidase: Friend and foe, *J. Leukocyte Biol. 77*, 598−625.
2. Nauseef, W. M., and Malech, H. L. (1986) Analysis of the peptide subunits of human neutrophil meyloperoxidase, *Blood 67*, 1504−1507.
3. Hurst, J. K. (1991) Myeloperoxidase: Active Site Structure and Catalytic Mechanisms, in *Peroxidases in Chemistry and Biology* (Everse, J., Everse, K., and Grisham, M. B., Eds.) 1st ed., pp 37−62, CRC Press, Boca Raton, FL.
4. Nauseef, W. M., Cogley, M., and McCormick, S. (1996) Effect of the R569W missense mutation on the biosynthesis of myeloperoxidase, *J. Biol. Chem. 271*, 9546−9549.
5. Dugad, L. B., La Mar, G. N., Lee, H. C., Ikeda-Saito, M., Booth, K. S., and Caughey, W. S. (1990) A nuclear Overhauser effect study of the active site of myeloperoxidase. Structural similarity of the prosthetic group to that on lactoperoxidase, *J. Biol. Chem. 265*, 7173−7179.
6. Taylor, K. T., Stroble, F., Yue, K. T., Ram, P., Pohl, J., Wood, A. S., and Kinkade, J. M., Jr. (1995) Isolation and identification

of a protoheme IX derivative released during autolytic cleavage of human myeloperoxidase, *Arch. Biochem. Biophys. 316*, 635−642.
7. Zeng, J., and Fenna, R. E. (1992) X-ray crystal structure of canine myeloperoxidase at 3 Å resolution, *J. Mol. Biol. 226*, 185−207.
8. Davey, C. A., and Fenna, R. E. (1996) 2.3 Å resolution X-ray crystal structure of the bisubstrate analogue inhibitor salicylhydroxamic acid bound to human myeloperoxidase: A model for a prereaction complex with hydrogen peroxide, *Biochemistry 35*, 10967−10973.
9. Fiedler, T. J., Davey, C. A., and Fenna, R. E. (2000) X-ray crystal structure and characterization of halide-binding sites of human myeloperoxidase at 1.8 Å resolution, *J. Biol. Chem. 275*, 11964−11971.
10. Blair-Johnson, M., Fiedler, T., and Fenna, R. (2001) Human myeloperoxidase: Structure of a cyanide complex and its interaction with bromide and thiocyanate substrates at 1.9 Å resolution, *Biochemistry 40*, 13990−13997.
11. Harrison, J. E., and Schultz, J. (1976) Studies on the chlorinating activity of myeloperoxidase, *J. Biol. Chem. 251*, 1371−1374.
12. Kettle, A. J., and Winterbourn, C. C. (1997) Myeloperoxidase: A key regulator of neutrophil oxidant production, *Redox Rep. 3*, 3−15.
13. Kettle, A. J., and Winterbourn, C. C. (1988) Superoxide modulates the activity of myeloperoxidase and optimizes the production of hypochlorous acid, *Biochem. J. 252*, 529−536.
14. Bolscher, B. G., and Wever, R. (1984) The nitrosyl compounds of ferrous animal haloperoxidases, *Biochim. Biophys. Acta 791*, 75−81.
15. Abu-Soud, H. M., and Hazen, S. L. (2000) Nitric oxide is a physiological substrate for mammalian peroxidases, *J. Biol. Chem. 275*, 37524−37532.
16. Abu-Soud, H. M., Khassawneh, M. Y., Sohn, J. T., Murray, P., Haxhiu, M. A., and Hazen, S. L. (2001) Peroxidases inhibit nitric oxide (NO) dependent bronchodilation: Development of a model describing NO-peroxidase interactions, *Biochemistry 40*, 11866−11875.
17. Galijasevic, S., Saed, G. M., Diamond, M. P., and Abu-Soud, H. M. (2003) Myeloperoxidase up-regulates the catalytic activity of inducible nitric oxide synthase by preventing nitric oxide feedback inhibition, *Proc. Natl. Acad. Sci. U.S.A. 100*, 14766−14771.
18. Abu-Soud, H. M., and Hazen, S. L. (2000) Nitric oxide modulates the catalytic activity of myeloperoxidase, *J. Biol. Chem. 275*, 5425−5430.
19. Abu-Soud, H. M., and Hazen, S. L. (2001) Interrogation of heme pocket environment of mammalian peroxidases with diatomic ligands, *Biochemistry 40*, 10747−10755.
20. Thayer, J. R., and Huffaker, R. C. (1980) Determination of nitrate and nitrite by high-pressure liquid chromatography: Comparison with other methods for nitrate determination, *Anal. Biochem. 102*, 110−119.
21. Rakita, R. M., Michel, B. R., and Rosen, H. (1990) Differential inactivation of *Escherichia coli* membrane dehydrogenases by a myeloperoxidase-mediated antimicrobial system, *Biochemistry 29*, 1075−1080.
22. Wever, R., Plat, H., and Hamers, M. N. (1981) Human eosinophil peroxidase: A novel isolation procedure, spectral properties and chlorinating activity. Kinetics of oxidation of tyrosine and dityrosine by myeloperoxidase compounds I and II. Implications for lipoprotein peroxidation studies, *FEBS Lett. 123*, 327−331.
23. Agner, K. (1963) Studies on myeloperoxidase activity, *Acta Chem. Scand. 17*, S332−S338.
24. Marquez, L. A., and Dunford, H. B. (1995) Kinetics of oxidation of tyrosine and dityrosine by myeloperoxidase compounds I and II. Implications for lipoprotein peroxidation studies, *J. Biol. Chem. 270*, 30434−30440.
25. Tahboub, Y. R., Galijasevic, S., Diamond, M. P., and Abu-Soud, H. M. (2005) Thiocyanate modulates the catalytic activity of mammalian peroxidases, *J. Biol. Chem. 280*, 26129−26136.
26. Galijasevic, S., Saed, G. M., Hazen, S. L., and Abu-Soud, H. M. (2006) Myeloperoxidase metabolizes thiocyanate in a reaction driven by nitric oxide, *Biochemistry 45*, 1255−1262.
27. Andrews, P. C., and Krinsky, N. I. (1982) A kinetic analysis of the interaction of human myeloperoxidase with hydrogen peroxide, chloride ions, and protons, *J. Biol. Chem. 257*, 13240−13245.
28. Harrison, J. E., and Schultz, J. (1976) Studies on the chlorinating activity of myeloperoxidase, *J. Biol. Chem. 251*, 1371−1374.
29. Wever, R., Kast, W. M., Kasinoedin, J. H., and Boelens, R. (1982) The peroxidation of thiocyanate catalysed by myeloperoxidase and lactoperoxidase, *Biochim. Biophys. Acta 709*, 212−219.
30. Bakkenist, A. R. J., De Boer, J. E. G., Plat, H., and Wever, R. (1980) The halide complexes of myeloperoxidase and the mechanism of the halogenation reactions, *Biochim. Biophys. Acta 613*, 337−348.
31. Araki, K., and Takeuchi, H. (2000) Effects of pH and chloride concentration on resonance Raman spectra of human myeloperoxidase and Raman microspectroscopic analysis of enzyme state in azurophilic granules, *Biopolymers 57*, 169−178.
32. Bolscher, B. G., and Wever, R. (1984) A kinetic study of the reaction between human myeloperoxidase, hydroperoxides and cyanide, inhibition by chloride and thiocyanate, *Biochim. Biophys. Acta 788*, 1−10.
33. Piciulon, P. L., Rupprecht, G., and Scheidt, R. W. (1974) Stereochemistry of nitrosylmetalloporphyrins. Nitrosyl-α,β,γ,δ-tetraphenylporphinato(1-methylimidazole)iron and nitrosyl-α,β,γ,δ-tetraphenylporphinato(4-methylpiperidine)manganese, *J. Am. Chem. Soc. 96*, 5293−5295.
34. Maxwell, J. C., and Caughey, W. S. (1976) An infrared study of NO bonding to heme B and hemoglobin A. Evidence for inositol hexaphosphate induced cleavage of proximal histidine to iron bonds, *Biochemistry 15*, 388−396.
35. Barlow, C., and Erecinska, M. (1979) Orientation of the NO ligand of cytochrome a_3 in nitrosyl cytochrome c oxidase, *FEBS Lett. 98*, 9−12.
36. Crane, B. R., Siegel, L. M., and Getzoff, E. D. (1997) Probing the catalytic mechanism of sulfite reductase by X-ray crystallography: Structures of the *Escherichia coli* hemoprotein in complex with substrates, inhibitors, intermediates, and products, *Biochemistry 36*, 12120−12137.
37. Bolognesi, M., Rosano, C., Losso, R., Borassi, A., Rizzi, M., Wittenberg, J. B., Boffi, A., and Ascenzi, P. (1999) Cyanide binding to *Lucina pectinata* hemoglobin I and to sperm whale myoglobin: An x-ray crystallographic study, *Biophys. J. 77*, 1093−1099.
38. Abu-Soud, H. M., Wu, C., Ghosh, D. K., and Stuehr, D. J. (1998) Stopped-flow analysis of CO and NO binding to inducible nitric oxide synthase, *Biochemistry 37*, 3777−3786.
39. Cooper, C. E. (1999) Nitric oxide and iron proteins, *Biochim. Biophys. Acta 1411*, 290−309.
40. Antonini, E., and Brunori, M. (1971) in *Hemoglobin and Myoglobin in Their Reactions with Ligands*, North-Holland Publishing Co., Amsterdam.
41. Cassoly, R., and Gibson, Q. H. (1975) Conformation, co-operativity and ligand binding in human hemoglobin, *J. Mol. Biol. 91*, 301−313.
42. Crane, B. R., Arvai, A. S., Gachhui, R., Wu, C., Ghosh, D. K., Getzoff, E. D., Stuehr, D. J., and Tainer, J. A. (1997) The structure of nitric oxide synthase oxygenase domain and inhibitor complexes, *Science 278*, 425−431.
43. Finzel, B. C., Poulos, T. L., and Kraut, J. (1984) Crystal structure of yeast cytochrome c peroxidase refined at 1.7-Å resolution, *J. Biol. Chem. 259*, 13027−13036.
44. Poulos, T. L., Edwards, S. L., Wariishi, H., and Gold, M. H. (1993) Crystallographic refinement of lignin peroxidase at 2 Å, *J. Biol. Chem. 268*, 4429−4440.
45. Sundaramoorthy, M., Kishi, K., Gold, M. H., and Poulos, T. L. (1994) The crystal structure of manganese peroxidase from *Phanerochaete chrysosporium* at 2.06-Å resolution, *J. Biol. Chem. 269*, 32759−32767.
46. Maroulis, G. (1993) Electric quadrupole moment and quadrupole polarizability of hydrogen bromide, *J. Phys. B: At., Mol. Opt. Phys. 26*, 2957−2964.
47. Kunishima, N., Fukuyama, K., Matsubara, H., Hatanaka, H., Shibano, Y., and Amachi, T. (1994) Crystal structure of the fungal peroxidase from *Arthromyces ramosus* at 1.9 Å resolution. Structural comparisons with the lignin and cytochrome c peroxidases, *J. Mol. Biol. 235*, 331−344.
48. Patterson, W. R., and Poulos, T. L. (1995) Crystal structure of recombinant pea cytosolic ascorbate peroxidase, *Biochemistry 34*, 4331−4341.
49. Schuller, D. J., Ban, N., van Huystee, R. B., McPherson, A., and Poulos, T. L. (1996) The crystal structure of peanut peroxidase, *Structure 4*, 311−321.
50. Bosshard, H. R., Anni, H., and Yonetani, T. (1991) Yeast Cytochrome c Peroxidase, in *Peroxidases in Chemistry and*

Biology (Everse, J., Everse, K. E., and Grisham, M. B., Eds.) Vol. II, pp 51−84, CRC Press, Boca Raton, FL.
51. Finzel, B. C., Poulos, T. L., and Kraut, J. (1984) Crystal structure of yeast cytochrome c peroxidase refined at 1.7 Å resolution, *J. Biol. Chem. 259*, 13027−13036.
52. Gajhede, M., Schuller, D. J., Henriksen, A., Smith, A. T., and Poulos, T. L. (1997) Crystal structure of horseradish peroxidase C at 2.15 Å resolution, *Nat. Struct. Biol. 4*, 1032−1038.
53. Mozzarelli, A., and Rossi, G. L. (1996) Protein function in the crystal, *Annu. Rev. Biophys. Biomol. Struct. 25*, 343−365.
54. Xu, W., Zheng, S., Dweik, R. A., and Erzurum, S. C. (2006) Role of epithelial nitric oxide in airway viral infection. *Free Radical Biol. Med. 41*, 19−28.
55. Brunetti, L., Francavilla, R., Tesse, R., Strippoli, A., Polimeno, L., Loforese, A., Miniello, V. L., and Armenio, L. (2006) Exhaled breath condensate pH measurement in children with asthma, allergic rhinitis and atopic dermatitis, *Pediatr. Allergy Immunol. 17*, 422−427.

BI0609725